AGU PUBLICATIONS

Geophysical Research Letters

RESEARCH LETTER
10.1002/2016GL068145

Key Points:
- Ionospheric bubble generation rates at two closely located longitudes can be very different
- Bubble generation obviously enhanced in more active ITCZ
- The enhanced generation can be explained by GWs in ITCZ that provide seeding source

Correspondence to:
G. Li,
gzlee@mail.iggcas.ac.cn

Citation:
Li, G., Y. Otsuka, B. Ning, M. A. Abdu, M. Yamamoto, W. Wan, L. Liu, and P. Abadi (2016), Enhanced ionospheric plasma bubble generation in more active ITCZ, *Geophys. Res. Lett.*, *43*, doi:10.1002/2016GL068145.

Received 6 FEB 2016
Accepted 7 MAR 2016
Accepted article online 10 MAR 2016

Enhanced ionospheric plasma bubble generation in more active ITCZ

Guozhu Li[1,2], Yuichi Otsuka[3], Baiqi Ning[1], M. A. Abdu[4,5], M. Yamamoto[6], Weixing Wan[1], Libo Liu[1], and Prayitno Abadi[3,7]

[1]Key Laboratory of Earth and Planetary Physics, Institute of Geology and Geophysics, Chinese Academy of Sciences, Beijing, China, [2]Beijing National Observatory of Space Environment, Institute of Geology and Geophysics, Chinese Academy of Sciences, Beijing, China, [3]Institute for Space-Earth Environmental Research, Nagoya University, Nagoya, Japan, [4]Instituto Nacional de Pesquisas Espaciais, Sao Jose dos Campos, Brazil, [5]Instituto Tecnologioc de Aeronautica, Sao Jose dos Campos, Brazil, [6]Research Institute for Sustainable Humanosphere, Kyoto University, Uji, Japan, [7]Space Science Center, Indonesian National Institute of Aeronautics and Space (LAPAN), Bandung, Indonesia

Abstract A close link between the atmospheric Intertropical Convergence Zone (ITCZ) and ionospheric plasma bubble has been proposed since the last century. But this relationship has often appeared to be less than convincing due to the simultaneous roles played by several other factors in shaping the global distribution of ionospheric bubbles. From simultaneous collaborative radar multibeam steering measurements at Kototabang (0.2°S, 100.3°E) and Sanya (18.4°N, 109.6°E), conducted during September–October of 2012 and 2013, we find that the total numbers of nights with bubble (i.e., occurrence rates) at the two closely located longitudes (Kototabang and Sanya) are comparable. But interestingly, the total number of nights with locally generated bubble (i.e., generation rate) over Kototabang is clearly more than that over Sanya. Further analysis reveals that a more active ITCZ is situated around the longitude of Kototabang. We surmise that the enhanced ionospheric bubble generation at Kototabang longitude could be caused by a higher gravity wave activity associated with the more active ITCZ.

1. Introduction

Ionospheric plasma bubbles producing scintillations can seriously affect satellite-based communication and navigation systems and are therefore of great practical interest. The bubbles, which mainly appear at equatorial and low latitudes, are known to result from instability process driven by the Rayleigh-Taylor (RT) fluid interchange mechanism [e.g., *Kelley*, 2009]. From earlier observations, we know that the evening prereversal enhancement of the eastward electric field (PRE) may control the instability growth rate and hence the global distribution of ionospheric bubbles [e.g., *Kil et al.*, 2009]. However, the role of another important factor responsible for the initiation of RT instability, the seeding source, is difficult to be identified and therefore still not well resolved [e.g., *Abdu*, 2001].

Theoretical and observational studies showed that the two factors, atmospheric gravity waves (GWs) and the PRE associated velocity shear, can act as seeds for the RT instability [e.g., *Huang and Kelley*, 1996; *Hysell and Kudeki*, 2004; *Abdu et al.*, 2009; *Patra et al.*, 2013]. By analyzing the longitudinal and seasonal variations of bubble occurrence and of the Intertropical Convergence Zone (ITCZ) indicated by the outgoing long-wave radiation (OLR) map, *McClure et al.* [1998] proposed that GWs generated in the ITCZ could initiate the RT instability and hence help explain the longitudinal distribution of ionospheric bubbles. *Ogawa et al.* [2006] correlated the occurrence of GPS scintillation produced by plasma bubbles with the OLR black body temperature in the longitude region of 80–100°E and found that the correlation coefficients varied in the range ±0.4. Later, *Tsunoda* [2010] extensively studied the correlations between ITCZ and ionospheric bubble. He suggested that GWs generated in ITCZ could play an important role in the development of bubbles during solstice. However, a more recent work by *Su et al.* [2014] showed that the relationship was not seen except at South American and African longitudes.

Due to the difficulty of identifying the bubble source location only with satellite in situ data, the longitude where bubble was observed (occurrence rate), instead of the longitude where bubble was locally generated (generation rate), was employed to investigate the correlation between the ITCZ and ionospheric bubble in earlier works [e.g., *Tsunoda*, 2010; *Su et al.*, 2014]. On the other hand, the GPS scintillation measurements over a given station cover a wide longitude region of more than 10° (with elevation angle $> 30°$). These could

produce mixed results while using different data sets since ionospheric bubble detected by satellite or GPS scintillation receiver could have traveled zonally more than 1000 km from their source longitudes before they are observed over any location [e.g., *Fukao et al.*, 2006; *Li et al.*, 2013a].

In this paper, we report the results from radar multibeam steering measurements simultaneously conducted at Kototabang (0.2°S, 100.3°E, dip latitude 10.4°S) and Sanya (18.4°N, 109.6°E, dip latitude 12.8°N) during September–October of 2012 and 2013, as part of a collaborative project to investigate the ionospheric bubble generation and its relationship to the ITCZ in Southeast Asia. Radar beam steering measurements can distinguish freshly generated bubbles in the longitude where the radar is located from those generated elsewhere that drifted into the radar beams [e.g., *Yokoyama et al.*, 2004]. Importantly, the two stations are separated only by 9.3° in longitude where the magnetic declination and the magnetic equator offset from the geographic equator are almost the same, so that the PRE does not change much between the two longitudes as that shown in earlier studies [e.g., *Batista et al.*, 1986; *Vichare and Richmond*, 2005; *Kil and Oh*, 2011]. The experimental results show for the first time that there exists an extremely large longitudinal variation in bubble generation but not in bubble occurrence. The bubble generation over Kototabang is found to be clearly higher than that over Sanya, whereas the bubble occurrence rates at the two stations are similar. Possible factors responsible for the extremely large longitudinal variation of the bubble generation rates are discussed.

2. Experiments

The Sanya VHF radar, with an operational frequency of 47.5 MHz and a peak power of 24 kW, can detect 3 m scale irregularities that occur in the ionospheric *E*, valley, and *F* regions [*Li et al.*, 2013b]. At Kototabang, there are two VHF radars operated at 30.8 MHz and 47 MHz, respectively, for 5 m and 3 m irregularities [e.g., *Fukao et al.*, 2006; *Otsuka and Effendy*, 2009]. The 47 MHz radar, i.e., the Equatorial Atmosphere Radar (EAR), has a peak power of 100 kW and has a beam steering capability on a pulse-to-pulse basis that permits detection of the spatial and temporal variations of the 3 m irregularities. Here we use the 47 MHz radar to investigate the ionospheric bubbles over Kototabang.

During September–October of 2012 and 2013, the Sanya and Kototabang radars were operated with 5-beam and 16-beam steering modes, respectively. Figure 1 shows the latitude-longitude locations and the beam directions (for details, please see Table 1 of *Li et al.* [2013a]) of the two radars. Due to the magnetic field-aligned characteristic of ionospheric bubbles [e.g., *Otsuka et al.*, 2002], the two radars, located in magnetically opposite hemispheres, can detect ionospheric bubbles generated around the magnetic equator that ascend to high enough altitudes. Notably, the ionospheric area scanned by the Sanya radar is smaller than that scanned by the Kototabang radar. For example, at an altitude of 300 km, the scanned areas by the two radars extend to about 280 km and 360 km in east-west direction, respectively. Here we use similar east-west width (as that indicated by shaded areas in Figure 1) to identify bubbles generated locally. It is evident from Figure 1 that the Kototabang radar can well distinguish the bubbles generated locally in the shaded area from those drifting zonally on the basis of the westernmost/easternmost beam measurements. Note that the westernmost and easternmost beams of the Kototabang (Sanya) radar were not (were) included in the shaded area. For the Sanya radar, if a bubble firstly appeared in the westernmost beam, the bubble could have two possibilities, generated locally near the westernmost beam or drifted from the western longitudes of the westernmost beam. On the basis of earlier multibeam steering observations that the initial generation of ionospheric bubbles exclusively appeared around or before apex sunset during equinox [*Yokoyama et al.*, 2004], if a bubble first appeared in the westernmost beam of shaded area before the apex sunset, the bubble will also be regarded as a locally generated bubble.

3. Results and Discussion

Figure 2 shows an example of ionospheric bubbles (backscatter plumes) detected by both radars on 11 October 2012. The backscatter echo profiles obtained from three beams of Kototabang and Sanya radars are shown in Figures 2 (left) and 2 (right), respectively. Over Kototabang, two bubble groups were observed around 12.5 and 14.5 UT (labeled A and B). The bubble group detected by the Sanya radar around 15 UT is labeled C. It can be noted that groups B and C appeared first in the westernmost beam and then in other beams. This indicates that the two groups of bubbles were generated in the western longitudes of the radar

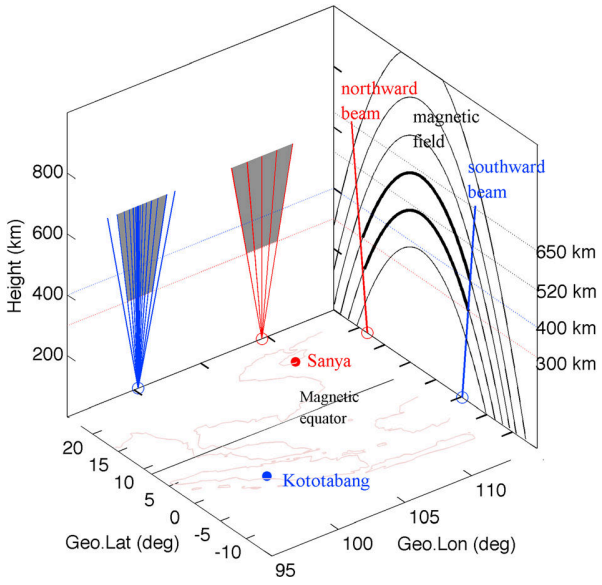

Figure 1. A schematic diagram showing geographic latitude-longitude locations and beam directions of Kototabang and Sanya radars. The radar-scanned area with shading shows the longitudes where bubbles were classified into two groups, generated locally and drifted from elsewhere.

site. They drifted eastward into and out of the radar-scanned area. For bubble group A, it was not detected in the west beam of Kototabang radar. Earlier studies over Kototabang and Sanya have suggested that such a beam-dependent bubble structure is generated locally around the longitude where the radar is located [e.g., *Yokoyama et al.*, 2004; *Li et al.*, 2012]. The present case of multibeam steering measurements clearly shows that on 11 October 2012, a locally generated ionospheric bubble was only detected at Kototabang longitude whereas zonally drifting bubbles were observed over both stations.

To determine the statistical behavior of ionospheric bubbles over Kototabang and Sanya, we investigated the simultaneous observations with the two radars during September–October of 2012 and 2013. Note that only geomagnetic quiet nights with daily averaged *Kp* less than 3 are considered in the statistical analysis. As shown in Figure 3, there is a total of 97 nights with simultaneous Kototabang and Sanya radar measurements (left blue bar). Out of these, we found 65 and 56 nights in which ionospheric bubbles were observed over Kototabang and Sanya, respectively. It is evident from the middle red and green bars that the bubble occurrence rates over the two stations (near 100°E and 110°E) are close (67% and 58%), showing consistent result with previous satellite in situ observations [e.g., *Kil et al.*, 2009]. While considering bubbles generated locally over radar longitudes, a significant difference is found between Kototabang and Sanya. As shown by the right red (green) bar, the number of nights with locally generated bubbles over Kototabang (Sanya) longitude is 52 (27), corresponding to the generation rate of 54% (28%). As a whole, the statistical analysis shows that the bubble generation rate is significantly higher (by about a factor of 2) at Kototabang longitude than it is over Sanya, whereas the bubble occurrence rates over the two stations are comparable.

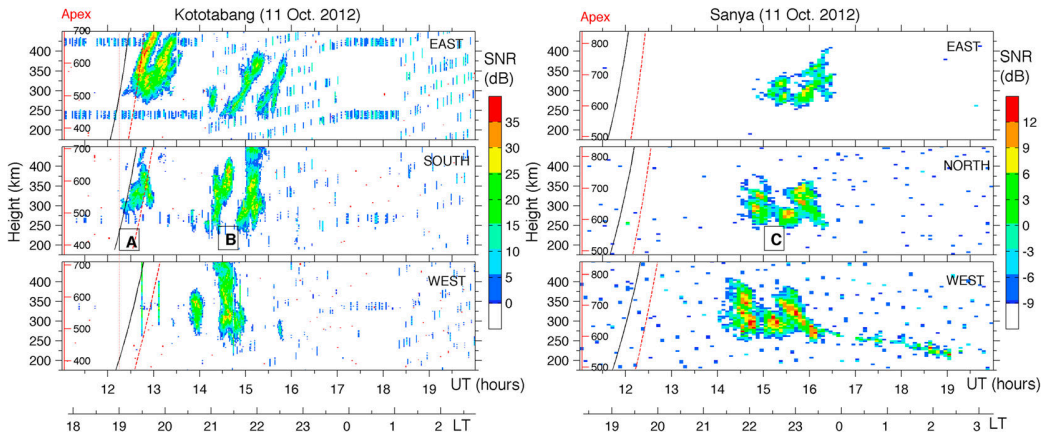

Figure 2. Height-time signal-to-noise ratio (SNR) plots of backscatter echo observed with (left) Kototabang and (right) Sanya radars on 11 October 2012. The apex altitude over magnetic equator (red vertical axis) and apex (red curve) and local (black curve) sunset terminators are superposed in each plot. The ionospheric bubble (backscatter plume) groups are marked with A to C.

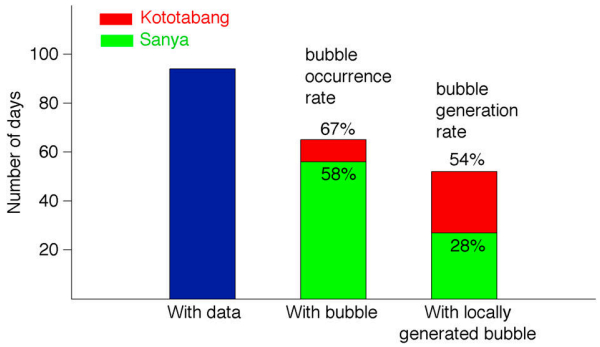

Figure 3. The number of days with simultaneous Kototabang and Sanya radar data (left bar), with bubbles (middle bar), and locally generated bubbles (right bar) over Kototabang and Sanya longitudes during September–October of 2012 and 2013. The corresponding percentage rates are also shown.

The question then arises as to what could cause the obvious difference between bubble generation rates over Kototabang and Sanya. Before discussing possible mechanisms responsible for the observed difference, we may note that the power aperture product of Kototabang radar is apparently higher than that of Sanya radar [e.g., *Fukao et al.*, 2006; *Li et al.*, 2012]. This, however, may not produce the significant difference of bubble generation over the two stations for the following reason. The VHF radar backscatter echo strength is proportional to the square of the density fluctuations, so that freshly generated bubbles (which are more turbulent with larger-density gradients) are more easily detected by a radar than are the zonally drifting (mostly in decaying process) bubbles. Statistically, the backscatter echo strength of ionospheric *F* region irregularities at later hours of the night is generally weaker than that of the freshly generated irregularities at postsunset hours [*Otsuka and Effendy*, 2009]. Therefore, if the radar power difference could produce the different bubble generation rates, it should cause much more difference between the bubble occurrence rates at the two stations. But that is not the case since the occurrence rates of bubbles detected by Sanya and Kototabang radars are comparable (Figure 3). On the other hand, we have also found several nights when locally generated bubble was simultaneously detected at both stations or only detected over Sanya, for example, the case shown in *Li et al.* [2013a]. Based on these considerations, it seems unlikely that the significant difference between bubble generation rates over Kototabang and Sanya can be attributed to the power difference of two radars.

Another difference between the two radars may concern their slightly different magnetic latitudes. As a result, an altitude of 300 km over Kototabang and Sanya corresponds to apex altitudes of ~520 km and ~650 km, respectively (Figure 1). If a bubble rises to apex altitudes of 520–650 km at the magnetic equator, it can be detected by Kototabang radar but may not be detected by the Sanya radar. This could cause a difference of bubble generation rates between the two stations. Through analyzing the maximum altitude of locally generated bubble (zonally drifting bubble) over Kototabang, we found that there are eight (nine) nights when the altitudes are less than 400 km (~650 km in apex altitude). If the lower altitude bubbles over Kototabang are not included in the statistical analysis, the bubble occurrence and generation rates will be 59% and 44%, respectively. In this way, the bubble occurrence rates at Kototabang and Sanya are nearly the same (59% and 58%), but the generation rates (44% and 28%) differ between them, obviously.

On the basis of earlier observational and theoretical model simulation studies [e.g., *Maruyama*, 1988; *Kelley*, 2009], we know that there are three primary factors that need to be considered in the bubble development process. These are (1) the PRE that raises the postsunset *F* layer to higher altitudes enhancing the growth rate of the RT instability, (2) a seeding source in the form of perturbations in density and polarization electric field needed to initiate the instability growth, and (3) meridional wind that can reduce polarization electric fields and thus impact negatively on the instability nonlinear growth to form bubble irregularities.

For the present observations performed at two longitudes (Kototabang and Sanya) separated only by 9.3°, the PRE could not vary much. For example, it is evident from earlier observations [e.g., *Kil and Oh*, 2011, Figure 4] and theoretical model simulations [e.g., *Vichare and Richmod*, 2005, Figure 3] that the evening peak vertical drifts at the two longitudes of 100°E (near Kototabang) and 110°E (near Sanya) are similar. Further, the Communication/Navigation Outage Forecast System (C/NOFS) evening vertical drift measurements during September–October of 2012 and 2013 demonstrate that the vertical drifts did not vary much in the longitudes of 100–110°E (figure not shown here). These results indicate that for the current study, the PRE is unlikely to cause any difference in the bubble generation efficiency/rate between Kototabang and Sanya longitudes. As regards the meridional wind, the results obtained from the HWM93 (horizontal wind model) model at the longitudes of Kototabang and Sanya are very similar (figure not shown here). However, we

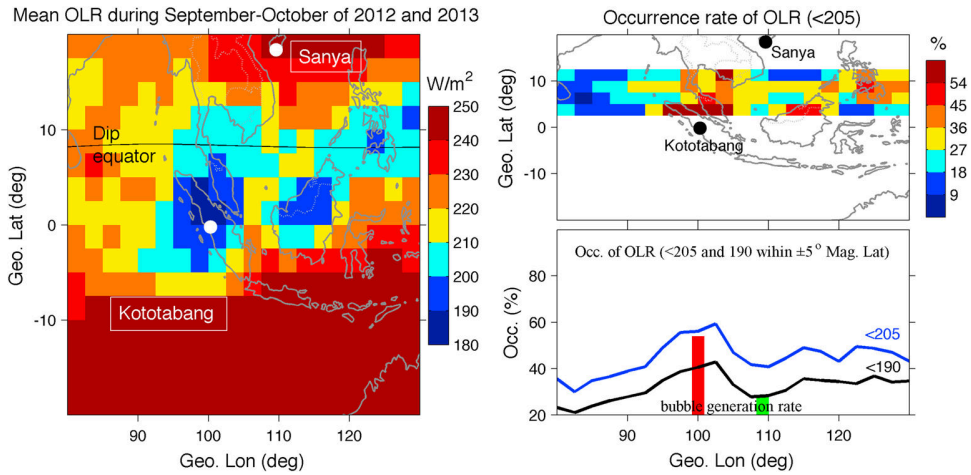

Figure 4. The longitudinal and latitudinal distributions of (left) mean outgoing long-wave radiation (OLR) and (right top) occurrence rate of OLR (<205). (right bottom) The longitudinal variations of averaged occurrence rates of OLR (<205 and 190) within ±5° magnetic latitude. The red and green bars show bubble generation rates over Kototabang and Sanya longitudes, respectively.

cannot exclude the possibility that the wind from HWM93 might not represent the real situation. If the significant differences of bubble generation rates were to be caused by meridional wind, it would require that stronger meridional winds be more frequent around 110°E (Sanya) than at 100°E (Kototabang), for which there is no evidence from observational or model studies.

We next investigate another factor, the seeding source. There are two types of sources that could serve as seeds for instability growth leading to plasma bubble generation. One is GW propagating upward from its generation source in tropospheric convective activity, which has long been hypothesized to seed the RT instability in theoretical simulations [e.g., *Huang and Kelley*, 1996] and observational studies [e.g., *Abdu et al.*, 2009; *Fritts et al.*, 2008]. The other has been suggested to be the velocity shear vortex that develops during the PRE period [*Kudeki and Bhattacharyya*, 1999]. Theoretical model simulations have shown that a velocity shear structure may be capable of seeding ionospheric bubble generation without requiring GW [e.g., *Hysell and Kudeki*, 2004]. Both GW and PRE associated velocity shear can produce the large-scale wave structure (LSWS) in the *F* region bottomside that has been demonstrated to be a necessary condition for ionospheric bubble generation [e.g., *Abdu et al.*, 2015; *Tsunoda*, 2015]. Using multi-instrument observations simultaneously performed at Kototabang and Sanya, *Li et al.* [2013a] reported a case where ionospheric bubble only appeared at Kototabang whereas satellite trace in ionograms indicative of LSWS was detected at both stations. In fact the plume pattern over Kototabang showed the presence of smaller-scale size structures (of the order of 50 km in east-west direction) imbedded in larger-scale sizes likely to be representative of the LSWS. Thus, multiple scales of wave structures with associated polarization electric fields were responsible for the generation of the entire plume patterns observed by the Kototabang radar. Based on these results, Li et al. proposed that besides the LSWS, there could be additional wave structures further intensifying the seeding process and helping/contributing to bubble generation over Kototabang. There is growing evidence that these wave structures are driven by a polarization electric field induced by GWs [*Abdu et al.*, 2015], and hence, we may expect their sources to be located in the convective activity associated with ITCZ.

In earlier studies on the statistical correlation between ionospheric bubbles and ITCZ, the daily OLR values were used [e.g., *McClure et al.*, 1998; *Tsunoda*, 2010; *Su et al.*, 2014]. Here we adopt a similar way as that used in the earlier studies to investigate if there is any relationship between the significantly enhanced bubble generation over Kototabang and the ITCZ. The interpolated OLR data obtained from the measurements of NOAA 18 are used. The equatorial daytime crossing time of the satellite is 1355 LT. *Gu and Zhang* [2002] reported that the ITCZ can be characterized with the OLR < 205 W/m^2. Smaller values of the OLR may be considered to be indicative of deeper convective activity. Figure 4 shows the distribution of the OLR during September–October of 2012 and 2013 in Southeast Asia. The latitude versus longitude distribution of the mean values of the OLR is presented in Figure 4 (left). Note that only the days with radar data are used.

We note in Figure 4 (left) that a group of small OLR values is present around the Kototabang longitude. At Sanya longitude, the area is dominated by relatively larger OLR values.

The OLR observations show that Kototabang is situated in a longitude of more active ITCZ, where deeper atmospheric convection could occur. Correspondingly, GWs could be generated through the convective system and propagate up to the thermosphere to induce ionospheric wave structure [*Tsunoda*, 2010]. In the work of *Su et al*. [2014], the frequency of OLR occurrences was employed to represent the frequency of GW occurrences. The wave structure, as mentioned above, can act as seeds of RT instability and thus lead to ionospheric bubble generation. *Tsunoda* [2010] reported that the GWs generated close to magnetic equator are more efficient in seeding the RT instability. Thus, we mainly focused on the OLR measurements around the magnetic equator. The latitude versus longitude distribution of the occurrence rate of OLR (within ±5° magnetic latitude) is presented in Figure 4 (right top). We defined the OLR occurrence rate in each grid (2.5° in longitude and latitude) as the number of days with OLR $<$ 205 in each grid divided by the total number of days (97). Figure 4 (right bottom) shows the longitudinal variation of the mean occurrence rate of OLR within ±5° magnetic latitude. Note that the OLR ($<$190) occurrence rate is also shown since *Su et al*. [2014] suggested that a well-defined threshold of OLR (with lower values) would help to assure the GW occurrence. It is evident from the panel that for both thresholds (190 and 205), the OLR occurrence rate is clearly higher at Kototabang longitude than at Sanya longitude. Correspondingly, the bubble generation rate (plotted as red and green vertical bars) is obviously higher over Kototabang than over Sanya, in excellent agreement with the OLR occurrences. This high degree of consistency suggests that the enhanced bubble generation at Kototabang longitude could be seeded by GWs originating from the more active ITCZ. Specifically, under weaker PRE condition, the strength of seeding is expected to play a more important role for initiating the bubble generation. *Abdu et al*. [2009] reported that for the PRE vertical drifts less than 30 m/s, the amplitude of the seeding perturbation required for the plasma instability growth was larger when the vertical drift was smaller. If the PRE associated vortex shear was not strong enough to seed the plasma instability at the longitudes of Kototabang and Sanya, the upward propagating GWs that could be generated more frequently in a more active ITCZ (near Kototabang longitude) might assist the seeding process and thus enhance bubble generation. By differentiating the bubbles generated locally from those drifted from elsewhere, we believe that our results indicate a close relationship between the enhanced bubble generation and active ITCZ.

4. Conclusions

With simultaneous Kototabang and Sanya radar multibeam steering measurements during September–October of 2012 and 2013, we have identified clear difference between bubble generation and occurrence rates over Sanya longitude and obvious difference between bubble generation rates at the two closely located longitudes (Kototabang and Sanya). The bubble generation rate over Kototabang was significantly enhanced compared with that over Sanya, whereas the bubble occurrence rates at the two stations were comparable. Meanwhile, the ITCZ in the longitude of Kototabang was more active (with a higher occurrence rate of low OLR value) and more closely located to magnetic equator than that in Sanya longitude. Based on earlier theoretical model simulation and satellite in situ observations of similar evening plasma vertical drifts over Kototabang and Sanya longitudes, we surmise that the PRE was unlikely to cause any difference in the bubble generation rate between the two longitudes. This, however, can be verified further with simultaneous observations of the PRE over the two longitudes on a daily basis in the future. Under the assumption of similar PRE at the two nearby longitudes, the enhanced bubble generation at Kototabang longitude could have been caused by a higher GW activity associated with the more active ITCZ, where the GWs could provide the seeding source for bubble development.

Acknowledgments

This research is supported by the National Natural Science Foundation of China (41422404, 41374163, 41321003, and 41374164), the Chinese Academy of Sciences (KZCX2-YW-Y10 and KZZD-EW-01-3), the National Important Basic Research Project of China (2012CB825604), and the International Joint Research Program of ISEE, Nagoya University. The Sanya radar data can be obtained on request from G.L. (gzlee@mail.iggcas.ac.cn) and B.N. (nbq@mail.iggcas.ac.cn). The Kototabang EAR radar is operated by RISH, Kyoto University, and LAPAN; the data can be obtained on request from M.Y. (yamamoto@rish.kyoto-u.ac.jp). The OLR data can be obtained at the website of NOAA (www.esrl.noaa.gov/psd/data/gridded/data.interp_OLR.html#plot). M.A.A. acknowledges the support from CAPES for a senior visiting professorship at ITA.

References

Abdu, M. A. (2001), Outstanding problems in the equatorial ionosphere thermosphere electrodynamics relevant to spread *F*, *J. Atmos. Sol. Terr. Phys.*, *63*, 869–884.

Abdu, M. A., E. Alam Kherani, I. S. Batista, E. R. de Paula, D. C. Fritts, and J. H. A. Sobral (2009), Gravity wave initiation of equatorial spread *F*/plasma bubble irregularities based on observational data from the SpreadFEx campaign, *Ann. Geophys.*, *27*, 2607–2622, doi:10.5194/angeo-27-2607-2009.

Abdu, M. A., J. R. de Souza, E. A. Kherani, I. S. Batista, J. W. MacDougall, and J. H. A. Sobral (2015), Wave structure and polarization electric field development in the bottomside *F* layer leading to postsunset equatorial spread *F*, *J. Geophys. Res. Space Physics*, *120*, 6930–6940, doi:10.1002/2015JA021235.

Batista, I., M. Abdu, and J. Bittencourt (1986), Equatorial *F* region vertical plasma drifts: Seasonal and longitudinal asymmetries in the American sector, *J. Geophys. Res.*, *91*(A11), 12,055–12,064, doi:10.1029/JA091iA11p12055.

Fritts, D. C., et al. (2008), Gravity wave and tidal influences on equatorial spread *F* based on observations during the Spread *F* Experiment (SpreadFEx), *Ann. Geophys.*, *26*, 3235–3252.
Fukao, S., T. Yokoyama, T. Tayama, M. Yamamoto, T. Maruyama, and S. Saito (2006), Eastward traverse of equatorial plasma plumes observed with the Equatorial Atmosphere Radar in Indonesia, *Ann. Geophys.*, *24*, 1411–1418, doi:10.5194/angeo-24-1411-2006.
Gu, G., and C. Zhang (2002), Cloud components of the Intertropical Convergence Zone, *J. Geophys. Res.*, *107*(D21), 4565, doi:10.1029/2002JD002089.
Huang, C. S., and M. C. Kelley (1996), Nonlinear evolution of equatorial spread *F*: 2. Gravity wave seeding of Rayleigh-Taylor instability, *J. Geophys. Res.*, *101*, 293–302, doi:10.1029/95JA02210.
Hysell, D. L., and E. Kudeki (2004), Collisional shear instability in the equatorial *F* region ionosphere, *J. Geophys. Res.*, *109*, A11301, doi:10.1029/2004JA010636.
Kelley, M. (2009), *The Earth's Ionosphere: Plasma Physics and Electrodynamics*, vol. 96, Elsevier, Academic Press, Boston, Mass.
Kil, H., and S.-J. Oh (2011), Dependence of the evening prereversal enhancement of the vertical plasma drift on geophysical parameters, *J. Geophys. Res.*, *116*, A05311, doi:10.1029/2010JA016352.
Kil, H., L. J. Paxton, and S.-J. Oh (2009), Global bubble distribution seen from ROCSAT-1 and its association with the evening prereversal enhancement, *J. Geophys. Res.*, *114*, A06307, doi:10.1029/2008JA013672.
Kudeki, E., and S. Bhattacharyya (1999), Postsunset vortex in equatorial *F* region plasma drifts and implications for bottomside spread-*F*, *J. Geophys. Res.*, *104*(A12), 28,163–28,170.
Li, G., B. Ning, M. A. Abdu, W. Wan, and L. Hu (2012), Precursor signatures and evolution of post-sunset equatorial spread-*F* observed over Sanya, *J. Geophys. Res.*, *117*, A08321, doi:10.1029/2012JA017820.
Li, G., B. Ning, M. A. Abdu, Y. Otsuka, T. Yokoyama, M. Yamamoto, and L. Liu (2013a), Longitudinal characteristics of spread *F* backscatter plumes observed with the EAR and Sanya VHF radar in Southeast Asia, *J. Geophys. Res. Space Physics*, *118*, 6544–6557, doi:10.1002/jgra.50581.
Li, G., B. Ning, A. K. Patra, M. A. Abdu, J. Chen, L. Liu, and L. Hu (2013b), On the linkage of daytime 150 km echoes and abnormal intermediate layer traces over Sanya, *J. Geophys. Res. Space Physics*, *118*, 7262–7267, doi:10.1002/2013JA019462.
Maruyama, T. (1988), A diagnostic model for equatorial spread *F*: 1. Model description and application to electric field and neutral wind effects, *J. Geophys. Res.*, *93*, 14,611–14,622, doi:10.1029/JA093iA12p14611.
McClure, J. P., S. Singh, D. K. Bamgboye, F. S. Johnson, and H. Kil (1998), Occurrence of equatorial *F* region irregularities: Evidence for tropospheric seeding, *J. Geophys. Res.*, *103*, 29,119–29,135.
Ogawa, T., Y. Otsuka, K. Shiokawa, A. Saito, and M. Nishioka (2006), Ionospheric disturbances over Indonesia and their possible association with atmospheric gravity waves from the troposphere, *J. Meteorol. Soc. Jpn.*, *84A*, 327–342.
Otsuka, Y., and T. O. Effendy (2009), VHF radar observations of nighttime *F*-region field-aligned irregularities over Kototabang, Indonesia, *Earth Planets Space*, *61*, 431–437.
Otsuka, Y., K. Shiokawa, T. Ogawa, and P. Wilkinson (2002), Geomagnetic conjugate observations of equatorial airglow depletions, *Geophys. Res. Lett*, *29*(15), 1753, doi:10.1029/2002GL015347.
Patra, A. K., A. Taori, P. P. Chaitanya, and S. Sripathi (2013), Direct detection of wavelike spatial structure at the bottom of the *F* region and its role on the formation of equatorial plasma bubble, *J. Geophys. Res. Space Physics*, *118*, 1196–1202, doi:10.1002/jgra.50148.
Su, S.-Y., C. Wu, and C. Liu (2014), Correlation between the global occurrences of ionospheric irregularities and deep atmospheric convective clouds in the Intertropical Convergence Zone (ITCZ), *Earth Planets Space*, *66*, 134.
Tsunoda, R. T. (2010), On seeding equatorial spread *F* during solstices, *Geophys. Res. Lett.*, *37*, L05102, doi:10.1029/2010GL042576.
Tsunoda, R. T. (2015), Upwelling: A unit of disturbance in equatorial spread *F*, *Prog. Earth Planet. Sci.*, *2*, 9, doi:10.1186/s40645-015-0038-5.
Vichare, G., and A. D. Richmond (2005), Simulation study of the longitudinal variation of evening vertical ionospheric drifts at the magnetic equator during equinox, *J. Geophys. Res.*, *110*, A05304, doi:10.1029/2004JA010720.
Yokoyama, T., S. Fukao, and M. Yamamoto (2004), Relationship of the onset of equatorial *F*-region irregularities with the sunset terminator observed with the Equatorial Atmosphere Radar, *Geophys. Res. Lett.*, *31*, L24804, doi:10.1029/2004GL021529.